BIOCHEMISTRY
including biophysical chemistry & molecular biology

Article

pubs.acs.org/biochemistry

Nanofluidity of Fatty Acid Hydrocarbon Chains As Monitored by Benchtop Time-Domain Nuclear Magnetic Resonance

Michelle D. Robinson[†,‡] and David P. Cistola*[,†,‡]

[†]Nanoparticle Diagnostics Research Laboratory, Division of Research & Innovation, and Department of Integrative Physiology, University of North Texas Health Science Center, Fort Worth, Texas 76107, United States

[‡]Departments of Clinical Laboratory Science and Biochemistry & Molecular Biology, College of Allied Health Sciences and Brody School of Medicine, East Carolina University, Greenville, North Carolina 27834, United States

Supporting Information

ABSTRACT: The functional properties of lipid-rich assemblies such as serum lipoproteins, cell membranes, and intracellular lipid droplets are modulated by the fluidity of the hydrocarbon chain environment. Existing methods for monitoring hydrocarbon chain fluidity include fluorescence, electron spin resonance, and nuclear magnetic resonance (NMR) spectroscopy; each possesses advantages and limitations. Here we introduce a new approach based on benchtop time-domain ^{1}H NMR relaxometry (TD-NMR). Unlike conventional NMR spectroscopy, TD-NMR does not rely on the chemical shift resolution made possible by homogeneous, high-field magnets and Fourier transforms. Rather, it focuses on a multiexponential analysis of the time decay signal. In this study, we investigated a series of single-phase fatty acid oils, which allowed us to correlate ^{1}H spin−spin relaxation time constants (T_2) with experimental measures of sample fluidity, as obtained using a viscometer. Remarkably, benchtop TD-NMR at 40 MHz was able to resolve two to four T_2 components in biologically relevant fatty acids, assigned to nanometer-scale domains in different segments of the hydrocarbon chain. The T_2 values for each domain were exquisitely sensitive to hydrocarbon chain structure; the largest values were observed for pure fatty acids or mixtures with the highest *cis*-double bond content. Moreover, the T_2 values for each domain exhibited positive linear correlations with fluidity. The TD-NMR T_2 and fluidity measurements appear to be monitoring the same underlying phenomenon: variations in hydrocarbon chain packing. The results from this study validate the use of benchtop TD-NMR T_2 as a nanofluidity meter and demonstrate its potential for probing nanofluidity in other systems of biological interest.

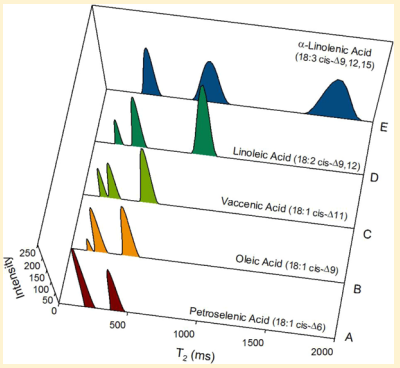

Lipids in biological systems display a remarkable variability in hydrocarbon chain composition, particularly in chain length and in the number, position, and stereochemistry of double bonds. That compositional variability underlies a considerable diversity in physical properties and biological functions.[1−5] For example, low-density lipoprotein (LDL), which functions as the primary cholesterol-carrying particle in the blood, undergoes a liquid-crystalline-to-liquid phase transition near body temperature.[6−11] Below this transition, the cholesteryl ester molecules in LDL pack in an ordered smectic liquid-crystalline phase, which makes LDL less fluid and more susceptible to oxidation and impaired clearance from the circulation.[12−15] The temperature at which this phase transition occurs depends on the fatty acyl composition of cholesteryl esters and triglycerides, which, in turn, is influenced by the dietary intake of saturated, mono- and polyunsaturated fatty acids.[16−22] Similarly, the hydrocarbon chain fluidity of biological membranes and membrane domains is thought to be a key determinant of cell surface receptor function.[23−34] For example, B-cell membrane lipid fluidity is altered through *n*−3 polyunsaturated fatty acid supplementation, which disrupts the lateral translocation of major histocompatibility complex class II into lipid rafts and suppresses T-cell activation.[35]

A variety of methods have been used to probe the fluidity of lipid-rich biological assemblies such as cell membranes, lipid droplets, and serum lipoproteins. Fluorescence and electron spin resonance methods have excellent sensitivity and have been used to characterize the rotational and lateral motions of a variety of lipid probes.[36−41] With the exception of parinaric acid found in exotic plants, biologically native fatty acids lack intrinsic fluorescence. Therefore, fluorescent probes such as DPH (1,6-diphenyl-1,3,5-hexatriene), NBD (nitrobenzoxadiazole), bis-pyrene, and BODIPY (4,4-difluoro-4-bora-3a,4a-diaza-*s*-indacene) have been synthetically incorporated into the fatty acid hydrocarbon chains of phospholipids and other lipids.[40,42] For electron spin resonance, fatty acid analogues incorporating a variety of spin-labels such as TEMPO [(2,2,6,6-tetramethylpiperidin-1-yl)oxyl] and doxyl moieties have been utilized.[37,43−46] While fatty acid analogues offer powerful tools

Received: September 19, 2014
Revised: November 18, 2014
Published: November 19, 2014

   dx.doi.org/10.1021/bi5011859 | *Biochemistry* 2014, 53, 7515−7522

for measuring probe dynamics, it is not clear what impact their non-native structures have on hydrocarbon chain packing in the vicinity of the probe. This potential complication can be avoided using nuclear magnetic resonance (NMR) spectroscopy, where ^{1}H, ^{2}H, or ^{13}C has been used to monitor hydrocarbon chain motions, order parameters, and/or fluidity.[47−53] Deuterium NMR is particularly well suited for studies of membranes, as it can be used to derive order parameters for hydrocarbon chains from quadrupolar splittings. However, it may not always be feasible or practical to incorporate ^{2}H into the biological system of interest; also, sensitivity can be a limiting factor. High-resolution ^{1}H and ^{13}C NMR spectroscopy is well suited for smaller assemblies such as serum lipoproteins and model membranes, including micelles, bicelles, and small unilamellar vesicles. However, the spectra of larger lipid assemblies like liposomes and cell membranes suffer from line broadening and poor chemical shift resolution.

Another source of uncertainty in studies of lipid fluidity is the ill-defined relationship between the properties of the spectroscopic probe and the actual fluidity of the lipid hydrocarbon chain environment. In strict terms, fluidity is defined as the inverse of viscosity that, in turn, is a measure of a fluid's resistance to flow.[54] There may be an implicit assumption that the spectroscopic or motional properties of a molecular probe are monitoring the fluidity of the lipid microenvironment. However, for that assumption to be rigorously validated, the spectroscopic or motional parameters should be calibrated against independent measures of fluidity.

Here we present a new approach for monitoring the nanofluidity of fatty acyl hydrocarbon chains using benchtop time-domain ^{1}H NMR (TD-NMR). In contrast to conventional Fourier transform NMR spectroscopy, which emphasizes analysis via the frequency domain, TD-NMR focuses on the exponential analysis of the time-domain signal. This type of NMR relaxometry (as opposed to spectroscopy) circumvents the requirement for superconducting magnets with a high magnetic field strength and field homogeneity. As a result, time-domain NMR can be performed on simpler, smaller, and less expensive benchtop instruments equipped with low-field permanent magnets. Thus, TD-NMR is more practical for use in non-NMR research laboratories, as well as in nonresearch settings, such as clinical diagnostic laboratories, manufacturing/quality control, and field testing sites. Moreover, it is better suited for the study of larger lipid membrane assemblies, as it does not rely on chemical shift resolution or narrow NMR resonances. While TD-NMR sacrifices the measurement of chemical shifts, it retains the ability to measure T_1 and T_2 relaxation time constants, which possess significant information content and resolving power on their own.

In this study, we utilized benchtop TD-NMR to resolve T_2 domains in a series of oil-phase fatty acids and biologically relevant fatty acid mixtures with varying hydrocarbon chain structures. The use of single-phase fatty acids afforded us the opportunity to correlate the TD-NMR values for hydrocarbon chain T_2 domains with independent measurements of sample fluidity. The results demonstrate the exquisite influence of hydrocarbon chain structure on T_2 and fluidity. These findings illustrate the potential of employing benchtop TD-NMR as a nanofluidity meter for analyzing a variety of biologically significant lipid, lipoprotein, and membrane assemblies. Moreover, this approach could help inform strategies for acquiring and interpreting T_2-weighted and -corrected MRI images of lipid-rich tissues,[55,56] as well as *in vivo* MRS analyses of hepatic lipid content in fatty liver disease.[57,58]

EXPERIMENTAL PROCEDURES

Sample Preparation. Individual neat fatty acids (>99% purity) were purchased from Nu-Chek Prep (Elysian, MN); for several of these samples, the purity was cross-checked and verified by ^{1}H and ^{13}C NMR spectroscopy. Free fatty acid-based fish oil extracts were kindly provided as a gift by Originates (Aventura, FL), a global supplier of omega-3 fish oil concentrates; they also provided a certificate of analysis for the sample composition and physical characteristics. The 7.5 mm diameter NMR tubes used for TD-NMR were filled to a sample volume of approximately 350 μL, corresponding to a sample height of 0.7 mm. The NMR tubes were evacuated with dry nitrogen gas before and after sample filling to minimize lipid oxidation during experiments. Most of the fatty acid samples used in this study showed no susceptibility to oxidation during multiple repeat experiments at ≥37 °C; the highly unsaturated α-linolenic (18:3), arachidonic (20:4), eicosapentaeneoic (20:5; EPA), and docosahexaeneoic (22:6; DHA) samples were more susceptible. For these fatty acids, each NMR experiment was performed within 2 h using a fresh sample.

Viscosity and Fluidity Measurements. The absolute viscosity values for single-phase fatty acid oil samples were measured using a VISCOlab 3000 instrument (Petroleum Analyzer Co. or PAC, L.P., Houston, TX). This laboratory viscometer utilizes a piston-style electromagnetic sensor, a Peltier-type temperature controller, and an integrated temperature sensor. In this study, two different pistons were employed, suitable for the absolute viscosity ranges of 0.5−10 and 10−200 cP. Each measurement utilized approximately 0.7 mL of fatty acid. Sample fluidity, reported here in units of inverse centipoise (cP^{-1}), was obtained by simply taking the inverse of the absolute viscosity.

Benchtop Time-Domain NMR Relaxometry. Measurements were acquired using a Bruker mq40 minispec NMR instrument equipped with a permanent magnet and operating at 0.94 T, corresponding to a resonance frequency of 40 MHz for ^{1}H. The magnet temperature on this particular instrument is controlled at 37 °C. This mq40 instrument is equipped with a 7.5 mm ^{1}H probe with variable sample temperature capability (Bruker probe model H40-7.5-15BAV) and a circulating water bath (Julabo, model F32-MA). To ensure sample temperature equilibration, the NMR samples were incubated in the instrument probe compartment at the experimental sample temperature at least 30 min before final NMR data acquisition was initiated.

Time-domain spin−spin relaxation exponential decay curves were acquired using a CPMG pulse sequence (Figure 1S of the Supporting Information) with a 2τ delay of 380 μs between 180° pulses, kept short to eliminate the potential impact of translational diffusion on T_2 values.[59,60] The 90° and 180° pulses were calibrated for each sample at each temperature prior to CPMG acquisition. The NMR intensities were acquired during the middle of the 2τ delays, and 4000−8000 data points were acquired for each decay curve, depending on the T_2. The recycle delay was set to $8T_1$ to ensure that the spins were fully relaxed at the beginning of the pulse sequence, and the data acquisition time was set to $8-9T_2$ so that the exponential decay curve reached the baseline. We observed that acquisition times significantly less than $8T_2$ resulted in poor resolution of the CONTIN-derived peaks in the T_2 profile. For

dx.doi.org/10.1021/bi5011859 | *Biochemistry* 2014, 53, 7515−7522

signal averaging, 512 scans were acquired for each experiment, corresponding to a total experiment time of ~2 h.

The multiexponential T_2 decay curves were analyzed using an inverse Laplace transform algorithm as implemented in CONTIN[61] (see also s-provencher.com). For oil-phase fatty acids, this analysis yielded two to four resolved T_2 exponential terms and the amplitudes associated with each term. The high signal-to-noise ratio obtained for oil-phase fatty acid samples provided sufficient information content in the data to ensure that the inverse Laplace calculations were stable and reproducible. The data are represented as T_2 profiles (intensity vs T_2).

This Bruker mq40 instrument is also equipped with a 10 mm ^{1}H probe that ultimately was not used in this study. We observed that T_2 decay curves acquired with the larger diameter probe for concentrated neat oil-phase fatty acid samples led to radiation damping. That phenomenon manifested itself as an oscillatory component in the residuals for the fit of the experimental data with the calculated CONTIN exponential decay curves. No such oscillations were observed when the smaller 7.5 mm probe was used, which has a sample volume that is approximately half that of the 10 mm probe.

NMR Spectroscopy. In this study, frequency-domain NMR spectroscopy was used for two purposes: (1) as an independent check of the T_2 domain assignments inferred from the time-domain NMR results and (2) as an independent check of the purity of the fatty acid samples obtained from Nu-Chek Prep, Inc. NMR spectra were recorded with a Magritek Spinsolve-Carbon benchtop NMR spectrometer operating at 1 T, corresponding to a resonance frequency of 42.5 MHz for ^{1}H and 10.8 MHz for ^{13}C. One-dimensional ^{1}H and ^{13}C spectra were acquired, and CPMG-based frequency-domain T_2 values were accumulated. Unlike the TD-NMR values, the T_2 curves in this case were generated by measuring the areas of resolved NMR resonances after Fourier transformation. In some cases, individual decay curves fit well to single exponentials, whereas in other cases, a biexponential fit was required, as analyzed with GraphPad Prism.

RESULTS

Fatty Acid T_2 Profiles and T_2 Assignments. The T_2 profiles for five different 18-carbon *cis*-unsaturated fatty acids, varying in the position and numbers of double bonds, are shown in Figure 1. Although T_2 profiles displayed in this manner (intensity vs T_2) bear a superficial resemblance to NMR spectra (intensity vs chemical shift), the two types of NMR data should not be confused with one another because they have a different *x*-axis and a fundamentally different meaning. The profiles displayed in this paper are inverse Laplace transforms of the multiexponential T_2 decay curves.

The first three T_2 profiles in Figure 1 correspond to fatty acids with a single *cis* double bond at positions Δ6, Δ9, and Δ11 (panels A–C, respectively). Petroselenic acid displays only two T_2 peaks, whereas oleic and vaccenic acids reveal three. As the position of the double bond moves away from the carboxyl group and closer to the methyl terminus, the peak at the lowest T_2 value increases in intensity (area under the peak). However, the T_2 values for the peaks are comparable for these three monounsaturated 18-carbon fatty acids. By contrast, the presence of a second and third *cis* double bond results in large increases in T_2 values, resulting in a dramatic right shift in the T_2 profiles for linoleic and α-linolenic acids (panels D and E, respectively).

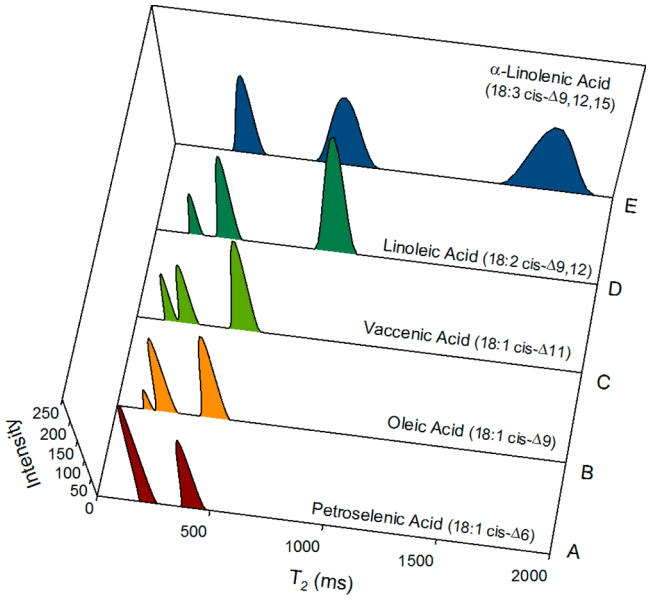

Figure 1. T_2 profiles for 18-carbon *cis*-unsaturated fatty acids at 37 °C showing the effect of double bond position and number for (A) petroselenic acid, 18:1 *cis*-Δ^6; (B) oleic acid, 18:1 *cis*-Δ^9; (C) vaccenic acid, 18:1 *cis*-Δ^{11}; (D) linoleic acid, 18:2 *cis*-$\Delta^{9,12}$; and (E) α-linolenic acid, 18:3 *cis*-$\Delta^{9,12,15}$.

The center of each resolved peak represents the average T_2 value for a domain or cluster of hydrogen atoms in the fatty acid molecule. The number of hydrogen atoms contributing to each domain, i.e., to each resolved T_2 peak, can be inferred from the relative amplitudes of the peaks derived from the inverse Laplace analysis. Oleic acid has a total of 34 hydrogen atoms and displayed a relative intensity ratio of ~3:18:13. Reasoning that the carboxyl proton is the least mobile because of intermolecular hydrogen bonding with the carboxyl group of an adjacent molecule,[3] we tentatively assigned the lowest T_2 domain to the three hydrogens at the carboxyl end, including the carboxyl proton and the C-2 methylene protons. The middle T_2 domain was assigned to the 18 hydrogen atoms in the middle of the hydrocarbon chain, spanning the double bond. The highest T_2 domain was assigned to the 13 distal hydrogen atoms, including the methyl terminus. These tentative assignments of the T_2 profile of oleic acid (Figure 2S and Table 1S of the Supporting Information) were subsequently confirmed using T_2 data from frequency-domain NMR spectroscopy (Figure 3S of the Supporting Information).

Effect of Hydrocarbon Chain Length on the T_2 Profile. Figure 2A–C displays T_2 profiles for three saturated fatty acids of increasing chain length: lauric (12:0), myristic (14:0), and palmitic acids (16:0), respectively. These data were acquired at 65 °C to ensure that all three fatty acids were above their crystalline-to-liquid phase transition and in the oil phase. Each of the saturated fatty acids displayed only two resolved T_2 domains. As hydrocarbon chain length increased, the T_2 values decreased, and the profile shifted to the left (Figure 2A–C). Moreover, the number of hydrogens in the lowest T_2 domain increased with increasing hydrocarbon chain length, while the protons in the higher T_2 domain remained constant (Table 1S of the Supporting Information).

Comparison of T_2 Profiles for Saturated and Monounsaturated Fatty Acids. Figure 2C–E compares palmitic acid with two of its monounsaturated counterparts, palmitoleic

dx.doi.org/10.1021/bi5011859 | Biochemistry 2014, 53, 7515–7522

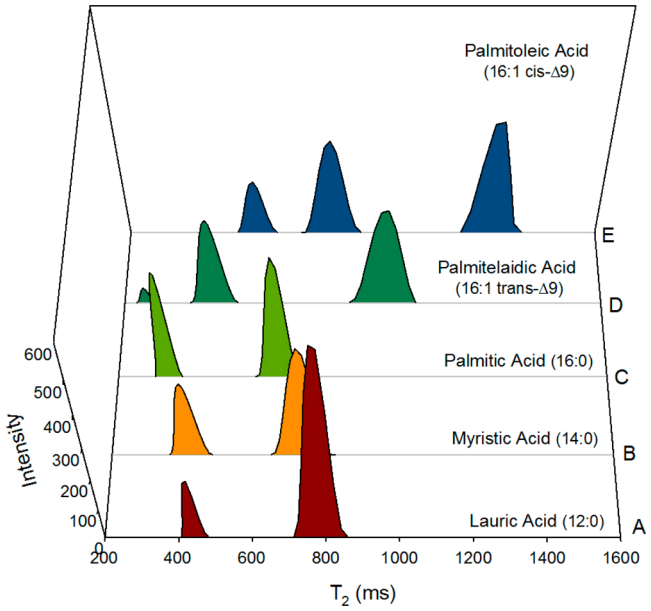

Figure 2. T_2 profiles for saturated and unsaturated fatty acids at 65 °C showing the effect of hydrocarbon chain length, saturation, and stereochemistry for (A) lauric acid, 12:0; (B) myristic acid, 14:0; (C) palmitic acid, 16:0; (D) palmitelaidic acid, 16:1 *trans*-Δ^9; and (E) palmitoleic acid, 16:1 *cis*-Δ^9.

(16:1 *cis*-Δ9) and palmitelaidic (16:1 *trans*-Δ9) acids. The addition of a double bond, regardless of the stereochemistry, increased the number of resolved T_2 domains from two to three. In addition, the T_2 values for 16-carbon fatty acids containing one double bond (Figure 2D,E) were both higher than that of the 16-carbon saturated fatty acid (Figure 2C).

Effect of Double Bond Stereochemistry. Two matched sets of monounsaturated fatty acids in their *cis* and *trans* configuration were compared: 16:1 *cis* and *trans* at 65 °C (Figure 2D,E and Table 1S of the Supporting Information) and 18:1 *cis* and *trans* at 55 °C (Table 1S of the Supporting Information). Each Δ9-monounsaturated fatty acid displayed three T_2 domains, although those with *cis* double bonds had much higher T_2 values than those with *trans* double bonds. Note that the T_2 values for fatty acids with a *trans* double bond were between those for *cis*-unsaturated and saturated fatty acids. The number of hydrogen atoms corresponding to each T_2 domain was only minimally affected by double bond stereochemistry (Table 1S of the Supporting Information).

Correlation of T_2 from TD-NMR with Sample Fluidity. Figure 3A displays the T_2 values for oleic acid measured across the temperature range of 25−55 °C. The results reveal a positive correlation of T_2 with temperature and with sample fluidity, as measured using a viscometer. All three resolved T_2 domains in oleic acid showed this positive correlation with fluidity. Similar positive correlations between NMR T_2 and bulk sample fluidity were observed for all three domains in palmitoleic acid (Figure 3B) and linoleic acid (Figure 3C).

To determine how hydrocarbon chain structure impacted the correlation between NMR T_2 and fluidity measurements, we compared values for a wide range of fatty acids that varied in hydrocarbon chain length, number of double bonds, and double bond stereochemistry, all at 37 °C. As shown in Figure 4, a positive correlation between TD-NMR T_2 and sample fluidity is apparent for each of the three resolved T_2 domains. Overall, the highest T_2 and fluidity values were observed for the fatty acids

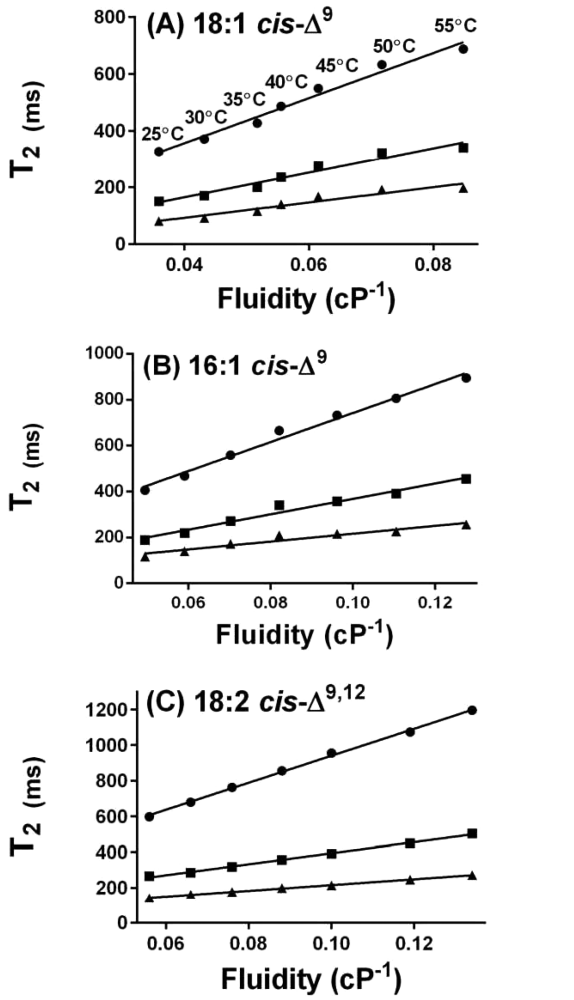

Figure 3. Temperature dependence of T_2 and fluidity for (A) oleic acid, (B) palmitoleic acid, and (C) linoleic acid. The temperatures shown above the points in panel A also pertain to the points shown in panels B and C: domain 1 (●), domain 2 (■), and domain 3 (▲). For oleic acid, the R^2 correlation coefficients for the plots are 0.99, 0.99, and 0.96 for domains 1−3, respectively. For palmitoleic acid, they are 0.99, 0.97, and 0.94, respectively. For linoleic acid, all three domains exhibit an R^2 value of 0.99.

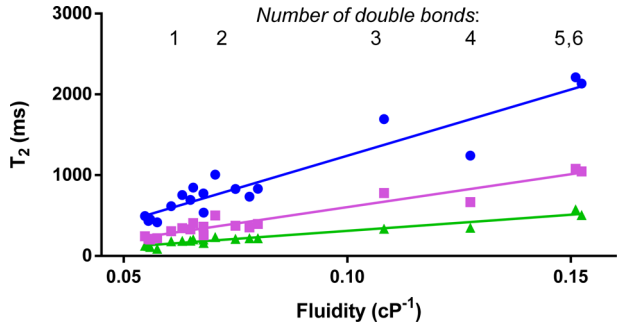

Figure 4. Correlation of T_2 with fluidity for a range of structurally distinct fatty acids and fatty acid mixtures at 37 °C. The blue curve represents data for domain 1, and the purple and green curves represent data for domains 2 and 3, respectively. The R^2 correlation coefficients for the plots of domains 1−3 were 0.90, 0.93, and 0.94, respectively.

with the largest numbers of double bonds. We reasoned that the deviation from linearity for α-linolenic and arachidonic

dx.doi.org/10.1021/bi5011859 | *Biochemistry* 2014, 53, 7515−7522

acids might be explained, in part, by the atypical hydrogen domain size (and hence average T_2) seen with those fatty acids. In this regard, the number of protons in domain 1 for α-linolenic acid is relatively low, in contrast to arachidonic acid, in which it is relatively high, compared to those of other fatty acids (Table 1S of the Supporting Information).

T_2 Profiles for Fatty Acid Mixtures. Binary mixtures of oleic and linoleic acids were prepared with varying percentages of the two components. As the volume percent of linoleic acid increased, so did the T_2 values and the fluidity for each domain at 37 °C (not shown).

To mimic the diversity of fatty acyl hydrocarbon chain structures seen in biological samples, we prepared oil-phase fatty acid mixtures with compositions similar to those seen in the human blood serum lipid profiles from individuals on a diet rich in saturated fats (SAFA), monounsaturated fats (MUFA), or polyunsaturated fats (PUFA).[20,21] The composition of these three mixtures is specified in Table 2S of the Supporting Information. The T_2 profiles are shown in Figure 5. Like pure linoleic acid, the mixtures showed four resolved T_2 components: three intense peaks and a very small peak at a low T_2 value. The PUFA mixture had the highest T_2 and fluidity values, whereas the SAFA mixture yielded the lowest. These results demonstrate that TD-NMR is able to detect differences in T_2 and fluidity in complex mixtures that mimic the variations in hydrocarbon chain composition seen in human blood serum.

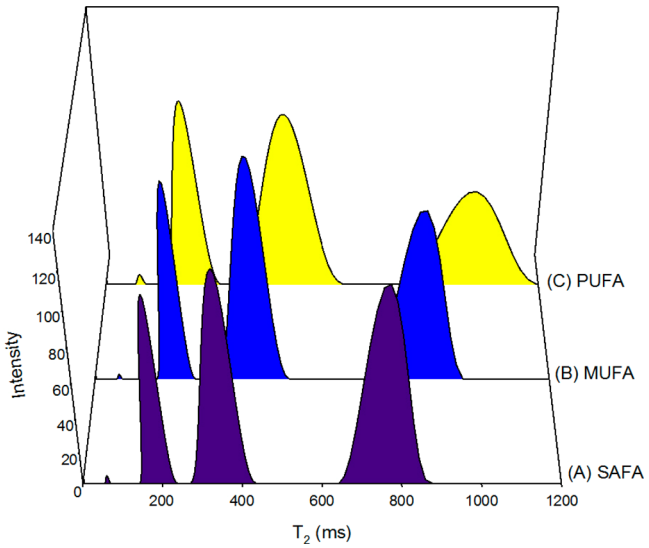

Figure 5. T_2 profiles at 37 °C for fatty acid mixtures that mimic serum lipid profiles for subjects on (A) a saturated fatty acid diet, (B) a monounsaturated fatty acid diet, and (C) a polyunsaturated fatty acid diet.[20,21] The composition of each fatty acid mixture is listed in Table 2S of the Supporting Information.

To assess the ability of benchtop TD-NMR to detect fluidity differences in nutritional oils, we compared two different free fatty acid-based fish oil samples highly enriched in $n-3$ ($\omega-3$) fatty acids. These two samples varied only slightly in the total percentage of $n-3$ fatty acids (74.8% vs 73.6%). The T_2 and fluidity values for the 74.8% $n-3$ sample were significantly higher (Figure 4S of the Supporting Information), consistent with the observation that $n-3$ fatty acids have the highest T_2 values (Figure 4). These results suggest that TD-NMR may be sensitive to small differences in hydrocarbon chain composition in nutritional oils.

DISCUSSION

The results from this study yielded three key observations. The first is that benchtop time-domain NMR is capable of resolving two to four T_2 domains in biologically relevant long chain fatty acids. These domains correspond to clusters of hydrogen atoms in the proximal (carboxyl), middle, and distal (methyl) segments of the hydrocarbon chain. This resolving power is remarkable, considering that benchtop TD-NMR relaxometry does not benefit from the chemical shift resolution afforded by conventional frequency-domain NMR spectroscopy. The second observation is that T_2 measurements are exquisitely sensitive to differences in hydrocarbon chain structure and composition. The most profound increases in T_2 were observed for individual fatty acids or mixtures with a higher content of *cis*-double bonds. The third key observation is that the average ^{1}H T_2 value for each molecular domain is linearly correlated with sample fluidity, as measured using a viscometer.

Molecular Origins of T_2 and Fluidity Differences. In principle, spin−spin or transverse relaxation time constants are able to probe molecular motions over a wide range of time scales.[62] Fast motions on the nanosecond-to-picosecond time scale include small-amplitude, high-frequency fluctuations such as segmental bond rotations or small-amplitude translational displacements.[63] Slow motions on the millisecond-to-second time scale involve large-amplitude fluctuations such as global conformational exchange or oligomerization in macromolecules. For the fatty acid systems studied here, we observed that T_2 is approximately equal to T_1 (extreme narrowing limit), implying that T_2 relaxation was driven primarily by fast motions with correlation times of $\ll$25 ns.

Upon comparison of T_2 values for domains within a given fatty acid molecule, the domain at the methyl end had average T_2 values higher than those of the middle and carboxyl domains. Thus, the hydrocarbon chain becomes progressively more mobile from the carboxyl end toward the methyl end, consistent with the notion that the carboxyl end is anchored by intermolecular hydrogen bonding. However, increasing the number of double bonds, which reduced the number of degrees of freedom for intramolecular bond rotations, had the effect of *increasing* the T_2 value, the opposite of what would be expected if intramolecular carbon−carbon bond rotations were the dominant contributors to fast Brownian motions. Instead, we propose that the dominant source of variation in the ^{1}H T_2 values measured in this study is variation in the interactions that occur between adjacent hydrocarbon chains.

Neat oil-phase fatty acids do not form ideal fluids but consist of small domains of hydrogen-bonded bilayers somewhat similar to the molecular organization seen in their X-ray crystal structures.[3,64] For saturated oil-phase fatty acids, the hydrocarbon chains pack quite tightly with low mean volumes per methylene group, especially near the carboxyl end. As demonstrated by J. A. Hamilton and D. M. Small, the ^{13}C T_1 values for oil-phase undecanoic acid, an 11-carbon saturated fatty acid, increase progressively from the carboxyl to the methyl end (Figures 8-26−8-28 of ref 3). For unsaturated fatty acids, the addition of a *cis*-double bond introduces a 120° kink into the chain, which is only partially overcome by trans−gauche isomerization in adjacent methylene groups. Hydrocarbon chain packing is disrupted, with a corresponding decrease in melting temperature. The increased volume per methylene group provides greater freedom for adjacent hydrocarbon chains to undergo molecular fluctuations. As

dx.doi.org/10.1021/bi5011859 | *Biochemistry* 2014, 53, 7515−7522

those fluctuations increase well above the Larmor frequency (here 40 MHz, corresponding to a 25 ns lifetime), T_2 and T_1 relaxation becomes less efficient and the relaxation time constants increase.

Molecular packing considerations may help explain the correlation between T_2 and fluidity as observed in this study. Viscosity, the inverse of fluidity, can be described as liquid friction. Such friction is increased by interactions between molecules. For oil-phase saturated fatty acids, those interactions include the van der Waals attractive forces between well-packed hydrocarbon chains. As *cis*-double bonds are introduced into the chain and the conformation becomes progressively more kinked and circular, chain packing weakens and van der Waals interactions weaken, resulting in less liquid friction and an increase in fluidity. Thus, the T_2 and fluidity measurements appear to be monitoring the same fundamental phenomenon, variations in hydrocarbon chain packing.

The relationship between T_2 and fluidity can also be explained using the generalized Stokes−Einstein−Debye relationship for rotational diffusion[65]

$$\tau_c^i = 1/D_r = \eta V f_i / k_B T \quad (1)$$

where τ_c^i is the rotational correlation time about the ith axis of a molecule in solution, D_r is the rotational diffusion constant, η is the absolute viscosity, V is the molecular volume, k_B is Boltzmann's constant, and T is the absolute temperature. The friction coefficient, f_i, is a dimensionless quantity that depends on the shape of the molecule and the boundary conditions imposed by the molecule and surrounding fluid. As fatty acid hydrocarbon chains have a dense network of spin-1/2 nuclei, the dominant relaxation mechanism is through dipole−dipole interactions.[62] The relationship between τ_c and T_2 for dipole−dipole relaxation is

$$1/T_2 = \gamma^2 \langle B^2 \rangle \{\tau_c + \tau_c/[1 + (2\pi\nu_o\tau_c)^2]\} \quad (2)$$

where γ is the gyromagnetic ratio for ^{1}H, $\langle B^2 \rangle$ is the mean square fluctuating field (the magnitude of the fluctuating field resulting from Brownian motion), and ν_o is the Larmor frequency.[63] In the extreme narrowing limit, where $T_2 = T_1$ and $(2\pi\nu_o\tau_c)^2 \ll 1$, eq 2 simplifies to

$$1/T_2 = \gamma^2 \langle B^2 \rangle 2\tau_c \quad (3)$$

Considering eqs 1−3 together leads to the following proportionality

$$T_2 \propto 1/\tau_c \propto D_r \propto 1/\eta \quad (4)$$

which predicts that T_2 should be inversely proportional to viscosity and directly proportional to fluidity. A similar proportionality holds for the Stokes−Einstein equation, which describes translational diffusion. Thus, the experimental observation of a linear relationship between T_2 and fluidity in this study provides evidence that these theoretical constructs are valid for the analysis of fatty acid hydrocarbon chains, at least for the systems studied here.

Measuring Nanofluidity in Other Biological Systems. The use of single-phase fatty acid oil samples permitted us to validate the correlation between ^{1}H T_2 and fluidity measurements and to establish T_2 from TD-NMR as a "nanofluidity meter". Similar T_2 measurements from benchtop TD-NMR could be used to measure nanofluidity in multiphase biological samples such as hydrated phospholipid bilayers, biological membranes, cell suspensions, or serum lipoproteins. All of those complex assemblies are bathed in an aqueous milieu, where measurements of bulk sample fluidity may not be relevant to the fluidity of the lipid nanoenvironment inside the membrane or lipoprotein assembly. In such complex samples, TD-NMR is able to probe what a viscometer cannot.

While ^{1}H T_2 measurements can be performed using conventional Fourier transform NMR spectroscopy, the benchtop TD-NMR relaxometry approach has several advantages. First, the time decay points are recorded directly during the delays embedded into the CPMG pulse scheme (Figure 1S of the Supporting Information). Therefore, the T_2 decay curve can be heavily sampled, allowing a more robust multiexponential analysis using inverse Laplace transforms. By contrast, the T_2 decay in NMR spectroscopy is assessed indirectly through the intensities obtained from a series of Fourier-transformed spectra. In practice, the T_2 decay curves from TD-NMR have 4000−8000 time points, whereas the corresponding curves from NMR spectroscopy typically have only approximately 10−50 points. A second advantage is that TD-NMR does not suffer from "line broadening" as seen in high-resolution ^{1}H or ^{13}C NMR spectroscopy of large membrane assemblies. Therefore, TD-NMR can be used to measure systems with short T_2 values, as it does not rely on resolving NMR resonances in the frequency domain. Like ^{2}H NMR, benchtop TD-NMR is particularly well suited for studying membranes and other large assemblies. A third advantage of benchtop TD-NMR is the relative simplicity and low cost of the instrumentation. It can be deployed in environments outside of the typical NMR research lab and should be more accessible to non-NMR specialists.

Finally, TD-NMR detects the properties of the ubiquitous hydrogen atom. There is no need to enrich molecules with ^{2}H or ^{13}C or to synthetically incorporate fluorescent or ESR probes into biological lipids. For all these reasons, benchtop TD-NMR shows promise for becoming a versatile tool for investigating lipid and membrane fluidity in a variety of samples of biological interest. Current efforts in our lab are focused on the application of TD-NMR to characterize lipoproteins in whole human serum from subjects with different metabolic disorders.

■ ASSOCIATED CONTENT

Supporting Information

Four figures and two tables. This material is available free of charge via the Internet at http://pubs.acs.org.

■ AUTHOR INFORMATION

Corresponding Author

*University of North Texas Health Science Center, 3500 Camp Bowie Blvd., EAD 858, Fort Worth, TX 76107. E-mail: david.cistola@unthsc.edu. Phone: (817) 735-2055.

Funding

This work was supported by institutional start-up funds from the University of North Texas Health Science Center and East Carolina University, as well as pilot grants from the East Carolina Diabetes and Obesity Institute and the Garvey Texas Foundation.

Notes

The authors declare no competing financial interest.

■ ACKNOWLEDGMENTS

D.P.C. dedicates this study to his former Ph.D. mentors, Profs. James A. Hamilton and Donald M. Small, who provided

education, enlightenment, and inspiration regarding NMR approaches to lipid and lipoprotein systems. We thank Drs. Bertram Manz and Hector Rodriguez of Magritek, Inc., for providing preliminary FT-NMR data for oleic acid from a Spinsolve benchtop NMR spectrometer prior to us purchasing the instrument. Also, we gratefully acknowledge the gift of fish oil extracts from Originates, Inc.

■ ABBREVIATIONS

CPMG, Carr−Purcell−Meiboom−Gill pulse sequence; DHA, docosahexaeneoic acid; EPA, eicosapentaeneoic acid; LDL, low-density lipoprotein; MRI, magnetic resonance imaging; MRS, magnetic resonance spectroscopy; MUFA, fatty acid mixture mimicking a diet rich in monounsaturated fatty acids; NMR, nuclear magnetic resonance; PUFA, fatty acid mixture mimicking a diet rich in polyunsaturated fatty acids; SAFA, fatty acid mixture mimicking a diet rich in saturated fatty acids; T_1, spin−lattice or longitudinal relaxation time constant; T_2, spin−spin or transverse relaxation time constant; TD-NMR, time-domain nuclear magnetic resonance.

■ REFERENCES

(1) Chapman, D. (1975) Phase transitions and fluidity characteristics of lipids and cell membranes. *Q. Rev. Biophys. 8*, 185−235.
(2) Small, D. M. (1984) Lateral chain packing in lipids and membranes. *J. Lipid Res. 25*, 1490−1500.
(3) Small, D. M. (1986) *The Physical Chemistry of Lipids: From Alkanes to Phospholipids*, Plenum Press, New York.
(4) Vance, D., and Vance, J., Eds. (2008) *Biochemistry of Lipids, Lipoproteins and Membranes*, Elsevier, Amsterdam.
(5) Thiam, A. R., Farese, R. V., Jr., and Walther, T. C. (2013) The biophysics and cell biology of lipid droplets. *Nat. Rev. Mol. Cell Biol. 14*, 775−786.
(6) Deckelbaum, R. J., Shipley, G. G., Small, D. M., Lees, R. S., and George, P. K. (1975) Thermal transitions in human plasma LDL. *Science 190*, 392−394.
(7) Atkinson, D., Deckelbaum, R. J., Small, D. M., and Shipley, G. G. (1977) Structure of human plasma low-density lipoproteins: Molecular organization of the central core. *Proc. Natl. Acad. Sci. U.S.A. 74*, 1042−1046.
(8) Zechner, R., Kostner, G. M., Dieplinger, H., Degovics, G., and Laggner, P. (1984) In vitro modification of the chemical composition of human plasma low density lipoproteins: Effects on morphology and thermal properties. *Chem. Phys. Lipids 36*, 111−119.
(9) Pregetter, M., Prassl, R., Schuster, B., Kriechbaum, M., Nigon, F., Chapman, J., and Laggner, P. (1999) Microphase separation in low density lipoproteins. Evidence for a fluid triglyceride core below the lipid melting transition. *J. Biol. Chem. 274*, 1334−1341.
(10) Prassl, R., and Laggner, P. (2009) Molecular structure of low density lipoprotein: Current status and future challenges. *Eur. Biophys. J. 38*, 145−158.
(11) Liu, Y., Lou, D., and Atkinson, D. (2011) Human LDL core cholesterol ester packing: Three-dimensional image reconstruction and SAXS simulation studies. *J. Lipid Res. 52*, 256−262.
(12) Schuster, B., Prassl, R., Nigon, F., Chapman, M. J., and Laggner, P. (1995) Core lipid structure is a major determinant of the oxidative resistance of low density lipoprotein. *Proc. Natl. Acad. Sci. U.S.A. 92*, 2509−2513.
(13) Morton, R., and Parks, J. S. (1996) Plasma cholesteryl ester transfer activity is modulated by the phase transition of the lipoprotein core. *J. Lipid Res. 37*, 1915−1923.
(14) McNamara, J. R., Small, D. M., Li, Z., and Schaefer, E. J. (1996) Differences in LDL subspecies involve alterations in lipid composition and conformational changes in apolipoprotein B. *J. Lipid Res. 37*, 1924−1935.
(15) Melchoir, J., Sawyer, J., Kelley, K., Shah, R., Wilson, M., Hantgan, R., and Rudel, L. L. (2013) LDL particle core enrichment in cholesteryl oleate increases proteoglycan binding and promotes atherosclerosis. *J. Lipid Res. 54*, 2495−2503.
(16) Kirchhausen, T., Untracht, S., Fless, G., and Scanu, A. (1979) Atherogenic diets and neutral-lipid organization in plasma low density lipoproteins. *Atherosclerosis 33*, 59−70.
(17) Pownall, H., Shepherd, J., Mantulin, W., Sklar, L., and Gotto, A. (1980) Effect of saturated and polyunsaturated fat diets on the composition and structure of human low density lipoproteins. *Atherosclerosis 36*, 299−314.
(18) Berlin, E., Judd, J., Marshall, M., and Kliman, P. (1987) Dietary linoleate increases fluidity and influences chemical composition of plasma low density lipoprotein in adult men. *Atherosclerosis 66*, 215−225.
(19) Nenseter, M., Rustan, A., Lund-Katz, S., Soyland, E., Maelandsmo, G., Phillips, M. C., and Drevon, C. A. (1992) Effect of dietary supplementation with n-3 polyunsaturated acids on physical properties and metabolism of low density lipoprotein in humans. *Arterioscler., Thromb., Vasc. Biol. 12*, 369−379.
(20) Nordöy, A., Hatcher, L. F., Ullmann, D. L., and Connor, W. E. (1993) Individual effects of dietary saturated fatty acids and fish oil on plasma lipids and lipoproteins in normal men. *Am. J. Nutr. 57*, 634−639.
(21) Sundram, K., Ismail, A., Hayes, K. C., Jeyamalar, R., and Pathmanathan, R. (1997) Trans (elaidic) fatty acids adversely affect the lipoprotein profile relative to specific saturated fatty acids in humans. *J. Nutr. 127*, 514−520.
(22) Callow, J., Summers, L., Bradshaw, H., and Frayn, K. (2001) Changes in LDL particle composition after the consumption of meals containing different amounts and types of fat. *Am. J. Clin. Nutr. 76*, 345−350.
(23) Spector, A., and Yorek, M. (1985) Membrane lipid composition and cellular function. *J. Lipid Res. 26*, 1015−1035.
(24) Lenaz, G. (1987) Lipid fluidity and membrane protein dynamics. *Biosci. Rep. 7*, 823−837.
(25) Hollan, S. (1996) Membrane fluidity of blood cells. *Haematologia 27*, 109−127.
(26) Clamp, A., Ladha, S., Clakc, D., Grimble, R., and Lund, E. (1997) The influence of dietary lipids on the composition and membrane fluidity of rat hepatocyte plasma membrane. *Lipids 32*, 179−184.
(27) Crane, J., and Tamm, L. (2004) Role of cholesterol in the formation and nature of lipid rafts in planar and spherical model membranes. *Biophys. J. 86*, 2965−2979.
(28) Mansilla, M., Cybulski, L., Albanesi, D., and Mendoza, D. (2004) Control of membrane lipid fluidity by molecular thermosensors. *J. Bacteriol. 186*, 6681−6688.
(29) Shaikh, R., and Edidin, M. (2006) Polyunsaturated fatty acids, membrane organization, T cells, and antigen presentation. *J. Clin. Nutr. 84*, 1277−1289.
(30) Sanchez, S., Tricerri, M., Ossato, G., and Gratton, E. (2010) Lipid packing determines protein-membrane interactions: Challenges for apolipoprotein A-1 and high density lipoproteins. *Biochim. Biophys. Acta 1798*, 1399−1408.
(31) Yang, X., Sheng, W., Sun, G., and Lee, J. (2011) Effects of fatty acid unsaturation numbers on membrane fluidity and α-secretase-dependent amyloid precursor protein processing. *Neurochem. Int. 58*, 321−329.
(32) Shaikh, R. (2012) Biophysical and biochemical mechanisms by which dietary N-3 polyunsaturated fatty acids from fish oil disrupt membrane lipid rafts. *J. Nutr. Biochem. 23*, 101−105.
(33) Calder, P. (2013) Fat chance to enhance B cell function. *J. Leukocyte Biol. 93*, 457−459.
(34) Nicolson, G. (2014) The fluid—mosaic model of membrane structure: Still relevant to understanding the structure, function and dynamics of biological membranes after more than 40 years. *Biochim. Biophys. Acta 1838*, 1451−1466.
(35) Rocket, B. D., Melton, M., Harris, M., Bridges, L. C., and Shaikh, S. R. (2013) Fish oil disrupts MHC class II lateral organization on the

B-cell side of the immunological synapse, independent of B-T cell adhesion. *J. Nutr. Biochem. 11*, 1810−1816.
(36) Vanderkooi, J., Fishkoff, S., Chance, B., and Cooper, R. A. (1974) Fluorescent probe analysis of the lipids architecture of natural and experimental cholesterol-rich membranes. *Biochemistry 13*, 1589−1595.
(37) Kveder, M., Pifat, G., Pecar, S., and Schara, M. (1994) The ESR characterization of molecular mobility in the lipid surface layer of human serum lipoproteins. *Chem. Phys. Lipids 70*, 101−108.
(38) Chochina, S. V., Avdulov, N. A., Igbavboa, U., Cleary, J. P., O'Hare, E. O., and Wood, W. G. (2001) Amyloid β-peptide1−40 increases neuronal membrane fluidity: Role of cholesterol and brain region. *J. Lipid Res. 42*, 1292−1297.
(39) Kahya, N., Scherfeld, D., Bacia, K., Poolman, B., and Schwille, P. (2003) Probing lipid mobility of raft-exhibiting model membranes by fluorescence correlation spectroscopy. *J. Biol. Chem. 278*, 28109−28115.
(40) Valeur, B., and Berberan-Santos, M. N. (2013) Microviscosity, Fluidity, Molecular Mobility. Estimation by Means of Fluorescent Probes. In *Molecular Fluorescence: Principles and Applications*, pp 226−245, John Wiley and Sons, New York.
(41) Hormel, T. T., Kurihara, S. Q., Brennan, M. K., Wozniak, M. C., and Parthasarathy, R. (2014) Measuring lipid membrane viscosity using rotational and translational probe diffusion. *Phys. Rev. Lett. 112*, 188101.
(42) Johnson, L., and Spence, M. (2010) Probes for Lipids and Membranes. In *Molecular Probes Handbook, A Guide to Fluorescent Probes and Labeling Technologies*, 11th ed., pp 549−579, Thermo Fisher Scientific Inc.
(43) Fretten, P., Morris, S. J., Watts, A., and Marsh, D. (1980) Lipid-lipid and lipid-protein interactions in chromaffin granule membranes. A spin label ESR study. *Biochim. Biophys. Acta 598*, 247.
(44) Crepeau, R. H., Saxena, S., Lee, S., Patyal, B., and Freed, J. H. (1994) Studies on lipid membranes by two-dimensional fourier transform ESR: Enhancement of resolution to ordering and dynamics. *Biophys. J. 66*, 1489−1504.
(45) Jurkiewicz, P., Olżyńska, A., Cwiklik, L., Conte, E., Jungwirth, P., Megli, F. M., and Hof, M. (2012) Biophysics of lipid bilayers containing oxidatively modified phospholipids: Insights from fluorescence and EPR experiments and from MD simulations. *Biochim. Biophys. Acta 1818*, 2388−2402.
(46) Mainali, L., Feix, J. B., Hyde, J. S., and Subczynski, W. K. (2011) Membrane fluidity profiles as deduced by saturation-recovery EPR measurements of spin-lattice relaxation times of spin labels. *J. Magn. Reson. 212*, 418−425.
(47) Hamilton, J. A., and Morrisett, J. D. (1986) Nuclear magnetic resonance studies of lipoproteins. *Methods Enzymol. 128*, 472−515.
(48) Seelig, A., and Seelig, J. (1974) Dynamic structure of fatty acyl chains in a phospholipid bilayer measured by deuterium magnetic resonance. *Biochemistry 13*, 4839−4845.
(49) Hakumäki, J. M., and Kauppinen, R. A. (2000) ^{1}H NMR-visible lipids in the life and death of cells. *Trends Biochem. Sci. 25*, 357−362.
(50) Orädd, G., Lindblom, G., and Westerman, P. W. (2002) Lateral diffusion of cholesterol and dimyristoylphosphatidylcholine in a lipid bilayer measured by pulsed field gradient NMR spectroscopy. *Biophys. J. 83*, 2702−2704.
(51) Larijani, B., and Dufourc, E. J. (2006) Polyunsaturated phosphatidylinositol and diacylglycerol substantially modify the fluidity and polymorphism of biomembranes: A solid-state deuterium NMR study. *Lipids 41*, 925−932.
(52) Brown, M. F., and Chan, S. I. (2007) Bilayer membranes: Deuterium and Carbon-13 NMR. *eMagRes*, DOI: 10.1002/9780470034590.emrstm0023.
(53) Leftin, A., and Brown, M. F. (2011) An NMR database for simulations of membrane dynamics. *Biochim. Biophys. Acta 1808*, 818−839.
(54) Schafer, T. (2009) Nearly perfect fluidity. *Physics 88*, 126001−126041.
(55) Corti, R., and Fuster, V. (2011) Imaging of atherosclerosis: Magnetic resonance imaging. *Eur. Heart J. 32*, 1709−1719.
(56) Meisamy, S., Hines, C. D. G., Hamilton, G., Sirlin, C. B., McKenzie, C. A., Yu, H., Brittain, J. H., and Reeder, S. B. (2011) Quantification of hepatic steatosis with T1-independent, T2*-corrected MR imaging with spectral modeling of fat: Blinded comparison with MR spectroscopy. *Radiology 258*, 767−775.
(57) Johnson, N. A., Walton, D. W., Sachinwalla, T., Thompson, C. H., Smith, K., Ruell, P. A., Stannard, S. R., and George, J. (2008) Noninvasive assessment of hepatic lipid composition: Advancing understanding and management of fatty liver disorders. *Hepatology 47*, 1513−1523.
(58) Gambarota, G., Tanner, M., van der Graaf, M., Mulkern, R., and Newbould, R. (2011) ^{1}H-MRS of hepatic fat using short TR at 3T: SNR optimization and fast T2 relaxometry. *Magn. Reson. Mater. Phys., Biol. Med. 24*, 339−345.
(59) Carr, H. Y., and Purcell, E. M. (1954) Effects of diffusion on free precession in nuclear magnetic resonance experiments. *Phys. Rev. 94*, 630−638.
(60) Meiboom, S., and Gill, D. (1958) Modified spin echo for measuring nuclear relaxation times. *Rev. Sci. Instrum. 29*, 688−691.
(61) Provencher, S. (1982) Contin: A general purpose constrained regularization program for inverting noisy linear algebraic and integral equations. *Comput. Phys. Commun. 35*, 229−242.
(62) Levitt, M. (2001) *Spin Dynamics: Basics of Nuclear Magnetic Resonance*, John Wiley & Sons, Ltd., New York.
(63) James, T. L. (1998) Fundamentals of NMR. In *Selected Topics in Biophysics*, pp 1−31, Biophysical Society, Rockville, MD.
(64) Cistola, D. P., Hamilton, J. A., Jackson, D., and Small, D. M. (1988) Ionization and phase behavior of fatty acids in water: Application of the Gibbs phase rule. *Biochemistry 27*, 1881−1888.
(65) Dote, J. L., and Kivelson, D. (1983) Hydrodynamic rotational friction coefficients for nonspheroidal particles. *J. Phys. Chem. 87*, 3889−3893.